Eur. Phys. J. A **9**, 213–220 (2000)

THE EUROPEAN PHYSICAL JOURNAL A

Role of multi-step processes in ^{16}O(^{11}B,^{12}C)^{15}N at 41.25 MeV

N. Ikeda[1,a], F. Nakamura[1], Y. Inotani[1], K. Koga[1], M. Koga[1], S. Koto[1], T. Sugimitsu[1], H. Fujita[2], and S. Morinobu[1]

[1] Department of Physics, Kyushu University, Fukuoka 812-8581, Japan
[2] Daiichi College of Pharmaceutical Sciences, Fukuoka 815-8511, Japan

Received: 3 July 2000 / Revised version: 4 September 2000
Communicated by D. Guerreau

Abstract. The ^{16}O(^{11}B,^{12}C)^{15}N reaction at 41.25 MeV has been investigated using the kinematical coincidence method. Polarization tensors t_{20} and t_{40} of ^{12}C[2^+_1] for the quantization axis taken along the direction of propagation have been measured at center-of-mass angles ($\Theta_{\rm c.m.}$) between 48° and 62° by analyzing the energy spectrum of ^{12}C[2^+_1] modulated by the effect of γ-ray emission. The cross-sections of the transfer reactions leading to the ^{12}C[g.s.]+^{15}N[g.s.], ^{12}C[2^+_1]+^{15}N[g.s.] and ^{12}C[g.s.]+^{15}N[$3/2^-_1$] final states have also been measured in the range $48^\circ \leq \Theta_{\rm c.m.} \leq 120^\circ$. The polarization tensor terms of ^{12}C[2^+_1] largely deviating from zero have been observed, contrary to the prediction by the distorted-wave Born approximation (DWBA). The one-step DWBA calculation also fails in describing the transfer reaction cross-sections. It is shown that the coupled channel model calculation including excitations and reorientations in ^{11}B and ^{12}C satisfactorily reproduces both the tensor terms and the cross-sections of the transfer reactions. The multi-step processes passing through the excited states of ^{11}B are found to significantly contribute to the reaction.

PACS. 25.70.Hi Transfer reactions – 24.70.+s Polarization phenomena in reactions – 24.10.Eq Coupled-channel and distorted-wave models

1 Introduction

The heavy-ion induced transfer reactions have been investigated for various colliding systems [1,2]. The angular distributions of the reaction cross-sections have generally been reproduced reasonably well by the distorted-wave Born approximation (DWBA) calculation. In some cases, however, the DWBA calculation has been pointed out to fail in reproducing the experimental data.

One of such examples can be seen in the ^{11}B+^{16}O $\rightarrow$^{12}C[2^+_1]+^{15}N[g.s.] reaction. Schlotthauer-Voos *et al.* [3] have indicated that the zero-range DWBA prediction significantly differs in the cross-section of the reaction at an ^{16}O incident energy of 60 MeV. The finite-range calculation has also been suggested to be unable to improve the reproducibility [4,5]. Modification of the optical potential parameters has been suggested [3] to give better description of the reaction data, though with a serious loss of reproducibility in the elastic scattering cross-sections.

To investigate the reaction mechanisms of the transfer reaction, it would be of special importance to examine such observables whose DWBA interpretation may not be obscured by the choice of the optical potential. The polarization tensors of the ejected particles meet this requirement in the case that the nuclear spin (I) of the ejectile is larger than the spin transfer (j) between the projectile and the ejectile [6]. This is because the one-step DWBA without the spin-dependent interactions predicts zero values for the tensors t_{kq}, with $2j < k \leq 2I$. The neglect of the spin-dependent interactions in the analysis of the heavy-ion induced reactions has generally been justified by the folding model which predicts the strengths to be negligibly small [7–9].

In the (^{11}B,^{12}C[2^+_1]) reaction, the most likely mechanism is one-step proton transfer process to the $p_{1/2}$ shell orbit in ^{12}C[2^+_1]. Since, in the absence of the spin-dependent interactions, the spin transfer j is equal to the total angular momentum of the orbit, the DWBA predicts non-zero values only for the vector terms. The proton transfer process to $p_{3/2}$ shell orbit, which is also allowed in the (^{11}B,^{12}C[2^+_1]) reaction, can produce non-zero tensor values for $k \leq 3$. Since, however, the spectroscopic factor of the $\pi(p_{3/2})\otimes^{11}$B[g.s.] configuration in ^{12}C[2^+_1] has been predicted to be two or three orders of magnitude smaller than that of $\pi(p_{1/2})\otimes^{11}$B[g.s.] [10,11], the $p_{3/2}$ proton transfer contribution would be negligible. Thus the DWBA theory is expected to predict zero value for the fourth rank tensors of ^{12}C[2^+_1] from (^{11}B,^{12}C[2^+_1]) and negligibly small values for the second rank ones.

The recent study of the tensor polarization in the ^{16}O(^{13}C,^{12}C[2^+_1])^{17}O reaction [6] has revealed that the fourth rank tensor term of ^{12}C[2^+_1] has a finite value, contrary to the one-step DWBA prediction for the $p_{3/2}$ shell

[a] e-mail: ikeda@kutl.kyushu-u.ac.jp

neutron stripping. In this case, the coupled channel (CC) model calculation, which takes into account excitations in ^{12}C and ^{13}C, has been successful in describing the measured polarization tensors as well as the cross-sections. The multi-step processes involving the excitations of ^{12}C and ^{13}C have been found to be important in reproducing the non-zero fourth rank tensor term of ^{12}C[2_1^+].

The multi-step processes passing through the excited states of ^{11}B and ^{12}C are similarly considered to contribute to the ^{16}O(^{11}B,^{12}C[2_1^+])^{15}N reaction. The experimental observation of the even rank polarization tensors of ^{12}C[2_1^+] from the ^{11}B+^{16}O reaction is, therefore, of great interest in examining the role of the multi-step processes. The cross-section data in a wide angular range would also be of help in verifying the assumed mechanisms.

In this paper, the experimental study of the ^{16}O(^{11}B, ^{12}C)^{15}N reaction at 41.25 MeV is presented. This incident energy was adopted to give the same center-of-mass (c.m.) energy with that of the experiment by Schlotthauer-Voos *et al.* [3]. The polarization tensors of t_{20} and t_{40} for ^{12}C[2_1^+], taking the quantization axis along the direction of propagation, were measured at c.m. scattering angles ($\Theta_{\rm c.m.}$) between 48° and 62° by analyzing the ^{12}C energy spectrum modulated by the effect of the γ-ray emission from the 2_1^+ state. The cross-section data of the transfer reactions leading to ^{12}C[g.s.]+^{15}N[g.s.], ^{12}C[2_1^+]+^{15}N[g.s.] and ^{12}C[g.s.]+^{15}N[$3/2_1^-$] covered the angular range of 48° $\leq \Theta_{\rm c.m.} \leq$ 120°. The elastic scattering cross-sections at $\Theta_{\rm c.m.}$ between 30° and 120° were also measured.

2 Experiment

Both the measurements of the polarization tensors of ^{12}C[2_1^+] and the cross-sections for the different final states in ^{12}C and ^{15}N were principally based on the kinematical coincidence method, where the ^{12}C nuclei and the ^{15}N recoils were detected in coincidence by two single-dimensional position-sensitive silicon detectors (PSDs). The coincidence events were recorded in a computer memory in a list mode and the desired ^{16}O(^{11}B,^{12}C)^{15}N data were constructed off-line with the aid of an appropriate event selection procedure. Since the raw data included all the coincidence events detected, the cross-sections of the ^{16}O(^{11}B,^{15}N)^{12}C and ^{16}O(^{11}B,^{16}O)^{11}B reactions and of the ^{11}B elastic scattering were also obtained from the same raw data by changing the event selection criteria. For the elastic scattering, an additional singles measurement was performed to determine the cross-sections at forward angles.

A target of SiO, evaporated onto a 20 μg/cm^2 thick carbon foil, was irradiated by a 41.25 MeV ^{11}B beam from the Kyushu University tandem accelerator, with the backing side facing the incident beam. In order to avoid the reduction in the efficiency of kinematical coincidence, the beam profile on the target was collimated to 1 mm in width and 2 mm in height, by placing a beam-defining baffle with an aperture of 3 mm ×2 mm at 247 mm upstream from the target. The ejected particles were measured by a 100 μm thick PSD (PSD-E) of 45 mm ×8 mm in area, placed 205 mm apart from the target, and the recoil nuclei by a 500 μm thick PSD (PSD-R) of the same effective area at 75 mm from the target.

In the measurement of the polarization tensors of ^{12}C[2_1^+], it was most important to assure, as discussed in [6], that all the ^{12}C nuclei detected by the PSD-E are in coincidence with the ^{15}N recoils in the PSD-R. For this purpose, the vertical acceptance angle of the PSD-E was defined by a slit of 36 mm ×2 mm in aperture, placed in front of the detector, whereas only the horizontal aperture of 30.4 mm was considered for the PSD-R. The angular ranges covered by the two detectors were 27.5° $\leq \theta_{\rm lab} \leq$ 36.5° (PSD-E) and −76.5° $\leq \theta_{\rm lab} \leq$ −53.6° (PSD-R). The target foil was tilted to make an angle of 70° to the beam to minimize the angular spread of ^{15}N due to multiple scattering in the target. For this geometry, the coincidence efficiency was estimated, by taking into account the effects of the finite beam width, the multiple scattering and the angular broadening by the γ-ray emission, to be no smaller than 99% for the ^{16}O(^{11}B,^{12}C[2_1^+])^{15}N[g.s.] reaction.

The cross-section data were collected in the above measurement as well as in a separate run with different settings of the detectors to cover ejectile angles between 36° and 55.5°. In the latter case, no detector slit was applied to the PSD-E and the target was set perpendicular to the beam direction. The data of the reactions leading to ^{12}C+^{15}N and ^{11}B+^{16}O were corrected by using the estimated kinematical coincidence efficiencies which ranged from 95% to 100% depending on the detection angle.

The oxygen thickness of the target was estimated to be 4.5 μg/cm^2 from the optical model analysis of the elastic scattering data at forward angles up to $\Theta_{\rm c.m.} = 50°$. In this estimation, the parameters of the Woods-Saxon type potential determined by Schotthauer-Voos *et al.* [3] were used. The measured elastic scattering angular distribution and the optical model prediction are displayed in fig. 1, together with the previous data [3] which have been obtained in a kinematically inverse condition to the present case. The agreement of both the data was found to be fair.

3 Data analysis

The individual reaction channels were satisfactorily identified by requiring the coincidence events to fall in the specified regions in the residue angle *vs.* ejectile angle and the residue energy *vs.* ejectile angle plots. The regions adopted for selection were determined following the prescription given in [6].

For each event of the ^{16}O(^{11}B,^{12}C)^{15}N reaction, the c.m. kinetic energy $E_{\rm c.m.}$ of ^{12}C was calculated from the ^{12}C detection angle $\theta_{\rm lab}$(^{12}C) and the ^{12}C detection energy, both of which were assumed to be correctly given by the measurement. Figure 2 shows the c.m. energy spectrum of ^{12}C from the ^{16}O(^{11}B,^{12}C)^{15}N reaction at $\theta_{\rm lab}$(^{12}C) = 32.0° ± 0.5°. The energy broadening of ^{12}C due to the γ-ray emission is clearly seen in the peak of the ^{16}O(^{11}B,^{12}C[2_1^+])^{15}N[g.s.] reaction.

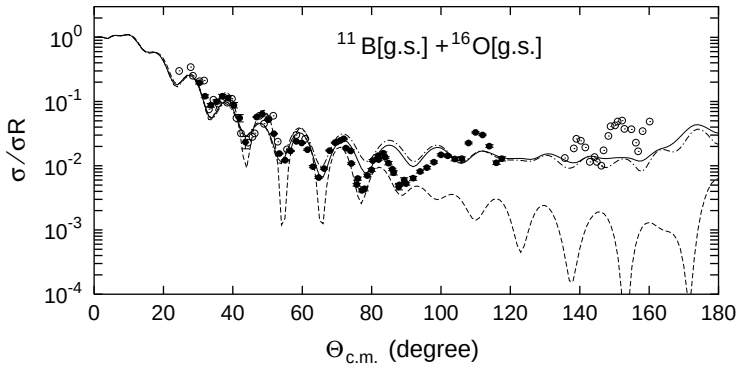

Fig. 1. Measured elastic scattering cross-sections of 41.25 MeV ^{11}B on ^{16}O (filled circles) and the previous data at the same center-of-mass energy from [3] (open circles), relative to the Rutherford value. The dashed line represents the optical model calculation. Also shown are the CC calculations with the negative (solid line) and positive (dot-dashed line) deformation lengths for excitations of ^{11}B.

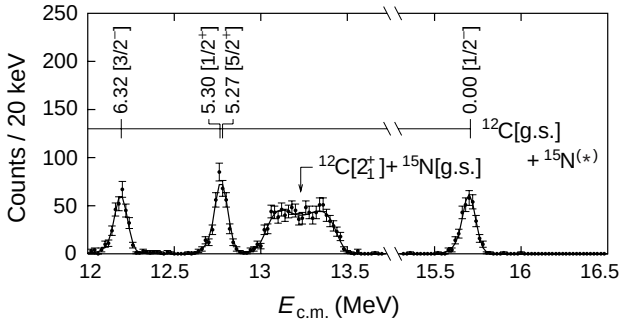

Fig. 2. Center-of-mass energy spectrum of ^{12}C for the ^{16}O(^{11}B,^{12}C)^{15}N reaction at $\theta_{\rm lab}(^{12}{\rm C}) = 32°$. The peaks are labeled by excitation energies (in MeV) and J^π of the final states in ^{15}N. The solid curve represents the fitted line shape (see text).

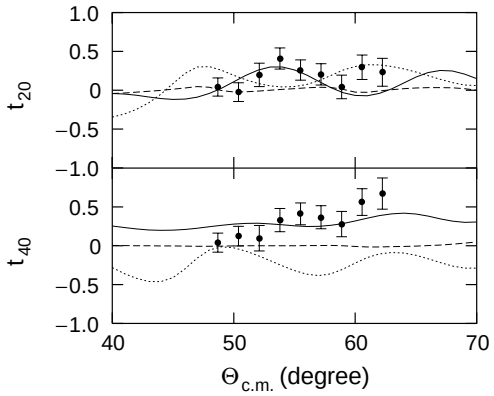

Fig. 3. Angular distributions of the polarization tensors t_{20} and t_{40} of ^{12}C[2$^+_1$] for the ^{16}O(^{11}B,^{12}C[2$^+_1$])^{15}N[g.s.] reaction. The dashed lines represent the DWBA calculation. The solid lines are the CC calculation (CC-I) with the negative deformation lengths for excitation of ^{11}B and the spectroscopic amplitudes listed in table 1. The CC calculation omitting the proton transfer processes to the excited states of ^{11}B is shown by the dotted lines.

According to [6], the double differential cross-section for the particles after the γ-ray emission is expressed in terms of the polarization tensor terms t_{kq} as

$$\frac{{\rm d}^2\sigma}{{\rm d}\Omega {\rm d}E_{\rm c}} = \frac{\sqrt{1-\beta_{\rm b}^2}}{2\beta_{\rm b}E_\gamma}\frac{{\rm d}\sigma}{{\rm d}\Omega}(\Theta)\sum_{k,{\rm even}} A_k t_{k0} P_k(\cos\theta_\gamma), \quad (1)$$

where $E_{\rm c}$ is the c.m. kinetic energy of the particle after the γ-ray emission, $\beta_{\rm b}$ the c.m. velocity of the particle before the γ-ray emission relative to the speed of light, Θ the c.m. detection angle, E_γ the energy of the emitted γ-ray and θ_γ the polar angle of the γ-ray emission measured from the z-axis taken along the direction of propagation of the particle before the γ-ray emission. The polar angle θ_γ is related to $E_{\rm c}$ by

$$\frac{\sqrt{1-\beta_{\rm b}^2}}{\beta_{\rm b}E_\gamma}(E_{\rm c}-E_{\rm b}) + \frac{1}{2}\beta_{\rm b} = -\cos\theta_\gamma,$$

where $E_{\rm b}$ is the c.m. kinetic energy before the γ-ray emission, which is uniquely determined by the two-body reaction kinematics. The tensor terms of t_{20} and t_{40} for ^{12}C[2$^+_1$] can be determined by analyzing the measured energy spectrum using (1).

The least-squares fit using the γ-recoil broadened line shape of (1), folded by the instrumental line profile, to the observed peak was carried out for each spectrum for the angle bin of 1° in the range of $\theta_{\rm lab}(^{12}{\rm C}) = 27.5°$–$36.5°$. The instrumental line shape was determined to reproduce both of the ^{12}C[g.s.]+^{15}N[g.s.] and ^{12}C[g.s.]+^{15}N[3/2$^-_1$] peak shapes, by assuming a Gaussian function with an exponential tail on the low-energy side. An example of the fits is shown in fig. 2 and the deduced t_{20} and t_{40} values against the c.m. scattering angle are presented in fig. 3.

Figure 4 shows the measured angular distributions of the cross-sections for the ^{16}O(^{11}B,^{12}C)^{15}N reaction. There are some differences between the present cross-sections and the previous data from [3] in the overlapping angular regions. As shown in fig. 2, the individual peaks of the transitions to ^{12}C[g.s.]+^{15}N[g.s.], ^{12}C[2$^+_1$]+^{15}N[g.s.], ^{12}C[g.s.]+^{15}N[1/2$^+_1$, 5/2$^+_1$] (unresolved) and ^{12}C[g.s.]+

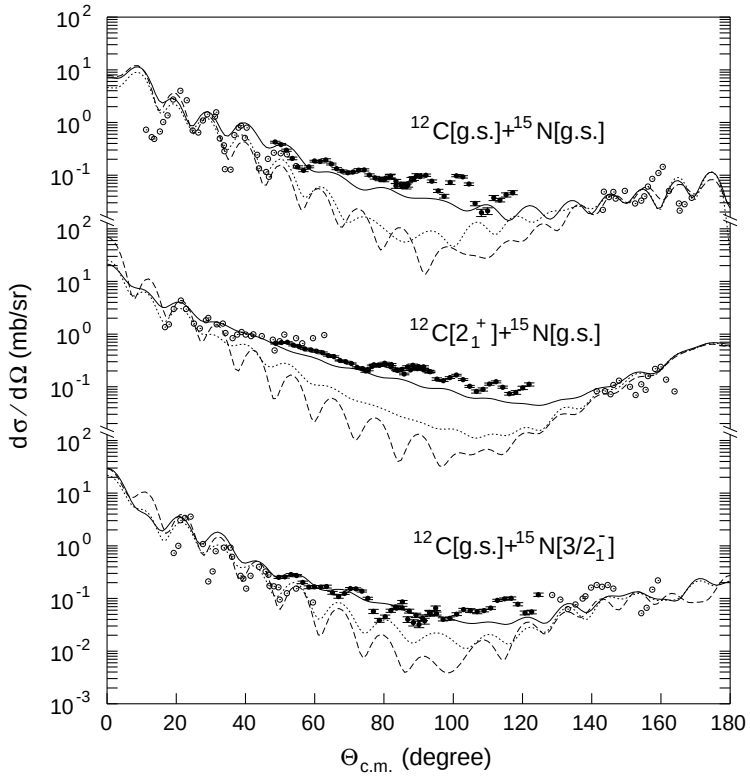

Fig. 4. Angular distributions of the cross-sections for ^{16}O(^{11}B,^{12}C)^{15}N at 41.25 MeV (filled circles) and the previous data (open circles) at the same center-of-mass energy from [3]. The dashed lines represent the DWBA calculations. The solid lines are the CC calculation (CC-I) with the negative deformation lengths for excitations of ^{11}B and the spectroscopic amplitudes listed in table 1. The CC calculation omitting the proton transfer processes to the excited states of ^{11}B is shown by the dotted lines.

^{15}N[3/2$_1^-$] were observed well isolated from each other in the present measurements. In the spectrum shown in [3], on the other hand, the peaks of ^{12}C[g.s.]+^{15}N[3/2$_1^-$] and ^{12}C[2$_1^+$]+^{15}N[g.s.] include significant contributions of the transitions to ^{12}C[g.s.]+^{15}N[1/2$_1^+$, 5/2$_1^+$], so that the inconsistencies for the transitions involving the excited states might be attributed to the possible error in the decomposition of the peaks in the previous data. Although the cause for the small difference in the transition to ^{12}C[g.s.]+^{15}N[g.s.] is not clear, the smaller cross-sections in the previous data might be suggestive of the presence of some counting loss.

4 Theoretical analysis

The experimental data were compared with the DWBA and CC calculations using a finite-range code FRESCO [12]. In both the calculations, the cross-sections and the polarization tensors were calculated, taking a coherent sum of proton and alpha-particle transfers into account. The internal wave functions of a proton and an alpha particle were calculated using the Woods-Saxon type potentials with $r = 1.25$ fm, $a = 0.65$ fm and $V_{\rm s.o.} = 6.0$ MeV, with the radius parameter r being multiplied by $A_{\rm core}^{1/3}$ for the proton case and by $4^{1/3}$+$A_{\rm core}^{1/3}$ for the alpha case, where $A_{\rm core}$ is the mass number of the core nucleus. The depths of the central potential were determined so as to reproduce the binding energies of the transferred particles.

4.1 DWBA analysis

The DWBA calculations were performed assuming that only the one-step transfer processes contribute to the reaction. The optical potential parameters of Woods-Saxon form in the incident and exit channels for ^{16}O(^{11}B,^{12}C[g.s.])^{15}N[g.s.] were taken from [3]. The parameter set (a) given for ^{16}O(^{11}B,^{12}C[2$_1^+$])^{15}N[g.s.] in [3] was used for the calculations of the reactions involving the excited states. The spectroscopic amplitudes of p+^{11}B and p+^{15}N were tentatively determined so as to roughly reproduce the previous data at forward angles [3], with fixing the p+^{11}B[g.s.] amplitudes in ^{12}C[2$_1^+$] at the values given by Cohen and Kurath [10]. The alpha-particle spectroscopic amplitudes were taken from [5]. The spectroscopic amplitudes used in the calculation are summarized in table 1, together with those used in the CC calculations (Sect. 4.2).

The calculated results of the angular distributions of the cross-sections for the reactions to ^{12}C[g.s.]+^{15}N[g.s.], ^{12}C[2$_1^+$]+^{15}N[g.s.] and ^{12}C[g.s.]+^{15}N[3/2$_1^-$] are shown by the dashed lines in fig. 4. Comparing the calculation with the previous data [3], the DWBA predictions are in reasonable agreement with the data for the (^{11}B,^{12}C[g.s.]) re-

Table 1. Spectroscopic amplitudes used for input data to the code FRESCO in the DWBA and CC calculations.

System	Orbit			Spectroscopic amplitude		
	n	l	j	DWBA	CC-I	CC-II
^{15}N[g.s.]+p $\rightarrow$^{16}O[g.s.]	0	1	1/2	1.753	1.300	1.300
^{15}N[3/2$^-_1$]+p $\rightarrow$^{16}O[g.s.]	0	1	3/2	2.479	1.600	1.600
^{11}B[g.s.]+p $\rightarrow$^{12}C[g.s.]	0	1	3/2	1.407	1.688	1.688
^{11}B[g.s.]+p $\rightarrow$^{12}C[2$^+_1$]	0	1	1/2	−0.741	−0.741	−0.741
^{11}B[g.s.]+p $\rightarrow$^{12}C[2$^+_1$]	0	1	3/2	−0.040	−0.040	−0.040
^{11}B[1/2$^-_1$]+p $\rightarrow$^{12}C[g.s.]	0	1	1/2		−0.868	0.868
^{11}B[3/2$^-_2$]+p $\rightarrow$^{12}C[g.s.]	0	1	3/2		−0.614	0.614
^{11}B[1/2$^-_1$]+p $\rightarrow$^{12}C[2$^+_1$]	0	1	3/2		0.800	−0.960
^{11}B[5/2$^-_1$]+p $\rightarrow$^{12}C[2$^+_1$]	0	1	3/2		1.300	−1.560
^{11}B[3/2$^-_2$]+p $\rightarrow$^{12}C[2$^+_1$]	0	1	3/2		−0.600	0.720
^{11}B[7/2$^-_1$]+p $\rightarrow$^{12}C[2$^+_1$]	0	1	3/2		−1.150	1.355
^{12}C[g.s.]+α $\rightarrow$^{16}O[g.s.]	2	0	0	−0.485	−0.485	−0.485
^{12}C[2$^+_1$]+α $\rightarrow$^{16}O[g.s.]	1	2	2	−0.350	−0.350	−0.350
^{11}B[g.s.]+α $\rightarrow$^{15}N[g.s.]	1	2	2	−0.637	−0.637	−0.637
^{11}B[g.s.]+α $\rightarrow$^{15}N[3/2$^-_1$]	2	0	0	0.728	0.728	0.728
^{11}B[g.s.]+α $\rightarrow$^{15}N[3/2$^-_1$]	1	2	2	−0.063	−0.063	−0.063

actions leading to the ground and 3/2$^-_1$ states of ^{15}N. Only for the transition to ^{12}C[2$^+_1$]+^{15}N[g.s.], a large discrepancy between the experiment and the calculation is observed. However, the angular distributions presently obtained in a wide angular range reveal that, for all of the three transitions, the calculated cross-sections decrease too rapidly relative to the experiment with increasing angles and become one or two orders of magnitudes smaller than the data at around $\Theta_{\rm c.m.} = 100°$.

The DWBA also fails in describing the experimental t_{20} and t_{40} values of ^{12}C[2$^+_1$], as shown in fig. 3. The contributions of the alpha transfer processes to the calculated tensor values were negligibly small as compared with the measured data.

Schlotthauer-Voos *et al.* [3] have demonstrated that a better agreement of the DWBA prediction with the experimental cross-sections can be obtained for the transition to ^{12}C[2$^+_1$]+^{15}N[g.s.] by changing the diffuseness parameter of the optical model potential. However, the non-vanishing t_{40} term clearly casts a question on the validity of this analysis, since the DWBA without the spin-dependent interactions predicts that the p shell nucleon transfer only produces finite t_{kq} values for $k \leq 3$, irrespective of the optical potentials adopted. The t_{20} values which significantly deviate from zero also support this claim, unless the spectroscopic amplitude of the $\pi(p_{3/2})\otimes^{11}$B[g.s] configuration relative to that of $\pi(p_{1/2})\otimes^{11}$B[g.s] in ^{12}C[2$^+_1$] is drastically increased from the value presently assumed.

4.2 CC analysis

The CC analyses were performed taking the coupling between the ground and 2$^+_1$ states in ^{12}C and the reorientation coupling in ^{12}C[2$^+_1$] into account. Also included were the couplings to the inelastic channels leading to four low-lying (1/2$^-_1$, 5/2$^-_1$, 3/2$^-_2$ and 7/2$^-_1$) states in ^{11}B, which are considered to be mainly of a $p_{3/2}$ shell proton hole coupled with a ^{12}C[2$^+_1$] core [11], and the reorientation coupling in ^{11}B[g.s.].

The ground and 2$^+_1$ states of ^{12}C were treated as members of a $K = 0$ band. For ^{11}B, the ground and excited states except the 1/2$^-_1$ one have been suggested to have $K = 3/2$ and 1/2 components with comparable magnitudes [13]. However, it has also been demonstrated in the ^{3}He+^{11}B [13] and ^{7}Li+^{11}B [14] collisions that the calculation without considering the K-band mixing reasonably describes the inelastic scatterings. Following the prescription in [13,14], the reorientation of ^{11}B[g.s.] and the transitions to the 5/2$^-_1$ and 7/2$^-_1$ states were calculated by assuming that the states have a unique K number of 3/2. For the excitations from the ground state to the 1/2$^-_1$ and 3/2$^-_2$ states, we assumed collective transitions in the $K =$ 1/2 band.

The deformation length for the reorientation of ^{11}B[g.s.] was obtained to be 1.88 fm from the quadrupole moment of ^{11}B[g.s.] reported in [15] and the ground state charge density from [16]. For the excitations of ^{11}B, the signs of the deformation lengths have not been decisively determined [13,14], so that the calculations were carried out for both the positive and negative deformation lengths. For the excitations to the 5/2$^-_1$ and 7/2$^-_1$ states, deformation lengths derived from the ^{7}Li+^{11}B inelastic scattering [14] were used. The same deformation length as that for the transition between the ground and 5/2$^-_1$ states was tentatively adopted for the excitations to the 1/2$^-_1$ and 3/2$^-_2$ states. The coupling parameters for ^{12}C were taken from [6]. The coupling parameters used in the CC calculations are summarized in table 2. The same de-

Table 2. Deformation lengths (in fm) used in the CC calculations.

^{11}B g.s. →g.s.	^{11}B g.s. →$1/2^-_1$	^{11}B g.s. →$5/2^-_1$	^{11}B g.s. →$3/2^-_2$	^{11}B g.s. →$7/2^-_1$	^{12}C g.s. →2^+_1	^{12}C 2^+_1 →2^+_1
+1.88	−1.20/+1.00	−1.20/+1.00	−1.20/+1.00	−1.65/+1.40	−1.48	−1.48

Table 3. Parameters of optical model potential of Woods-Saxon form used in the CC calculations.

System	V (MeV)	r_R (fm)	a_R (fm)	W (MeV)	r_I (fm)	a_I (fm)
^{11}B+^{16}O	46.0	1.200	0.600	4.4	1.360	0.400
^{12}C+^{15}N	55.0	1.214	0.484	8.0	1.348	0.250

formation lengths were used for the nuclear and Coulomb deformations.

The optical potential parameters of Woods-Saxon form for ^{11}B+^{16}O were determined so as to reproduce the measured elastic scattering cross-sections. As shown in fig. 1, both of the CC calculations with opposite signs of the deformation lengths for the excitations of ^{11}B reasonably describe the elastic scattering data for the same optical potential parameters. It is to be noted in this figure, that the CC calculations agree in magnitude with the measured elastic scattering cross-sections at $\Theta_{\rm c.m.} \geq 90°$ and the previous data at backward angles [3] where the optical model calculation is not successful. The structure in the experimental angular distribution in the backward angular region, which could not be reproduced by the present CC calculations, might have the origin in the effect of the elastic transfer process [5]. For the ^{12}C+^{15}N system, the elastic scattering data at around the present c.m. energy ($E_{\rm c.m.} = 28.27$ MeV) have not been available. We therefore determined the optical potential parameters from the CC analysis of the ^{12}C+^{14}N elastic scattering cross-sections at $E_{\rm c.m.} = 30$ MeV from [17]. The optical potential parameters used in the CC calculations are summarized in table 3.

The proton transfer processes to the excited states of ^{11}B were taken into account in the calculation, whereas those of alpha particle transfer, which are only considered to contribute to ^{16}O(^{11}B,^{12}C)^{15}N at backward angles, were not included. The spectroscopic amplitudes of p+^{11}B and p+^{15}N were so adjusted to reproduce the experimental data with fixing the amplitudes of p+^{11}B[g.s.] in ^{12}C[2^+_1] and the magnitudes of the p+^{11}B[$1/2^-_1$] and p+^{15}N[$3/2^-_2$] amplitudes in ^{12}C[g.s.] at the values given by Cohen and Kurath [10]. The same spectroscopic amplitudes with the DWBA calculation (Sect. 4.1) were used for the alpha particle transfer processes.

The results of the calculation with the negative deformation lengths for the excitations of ^{11}B (CC-I) are shown by the solid lines in figs. 3 and 4. The calculation with the spectroscopic amplitudes given in table 1 (CC-I) reasonably describes the polarizations tensors of t_{20} and t_{40} for ^{12}C[2^+_1] as well as the cross-sections for the transitions to ^{12}C[g.s.]+^{15}N[g.s.], ^{12}C[2^+_1]+^{15}N[g.s.] and ^{12}C[g.s.]+^{15}N[$3/2^-_1$].

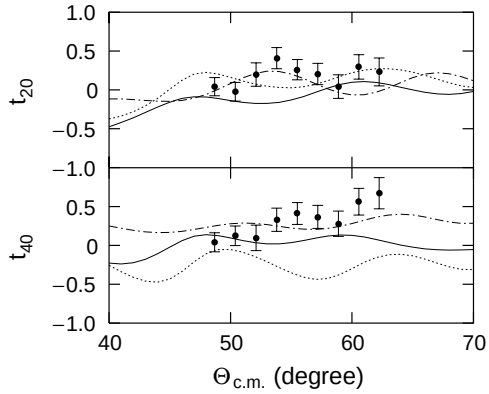

Fig. 5. CC calculations of the tensor terms of ^{12}C[2^+_1] with the positive deformation lengths for excitations of ^{11}B, applying the spectroscopic amplitudes listed in columns CC-I (solid lines) and CC-II (dot-dashed lines) in table 1, and the calculation omitting the proton transfer processes to the excited states of ^{11}B (dotted lines).

The calculations (CC-II) with the positive deformation lengths for the excitations of ^{11}B were also carried out. We first adopted the same spectroscopic amplitudes with the CC-I calculation. The results are shown by the solid lines in figs. 5 and 6. The calculation reproduces the cross-sections as reasonably well as that with the negative deformation lengths, except for the transition to ^{15}N[$3/2^-_1$]. However, the prediction of the calculation for the polarization tensors was rather poor. We further examined the signs of the p+^{11}B* spectroscopic amplitudes in ^{12}C[g.s.] and ^{12}C[2^+_1], with fixing the magnitudes at the values adopted in CC-I. The signs of the spectroscopic amplitudes were found necessary to be reversed from those in CC-I to reproduce the tensor terms of ^{12}C[2^+_1] (not shown in the figure). Since, however, the calculation still gave a somewhat worse description of the data than CC-I, we further performed the calculations with different magnitudes of the spectroscopic amplitudes of p+^{11}B* in ^{12}C[2^+_1]. It was found that the calculation with the spectroscopic amplitudes given in column CC-II in table 1 describes both the polarization tensors and the cross-sections as reasonably well as the calculation with the negative deformation lengths. The results of the calculation are shown by the

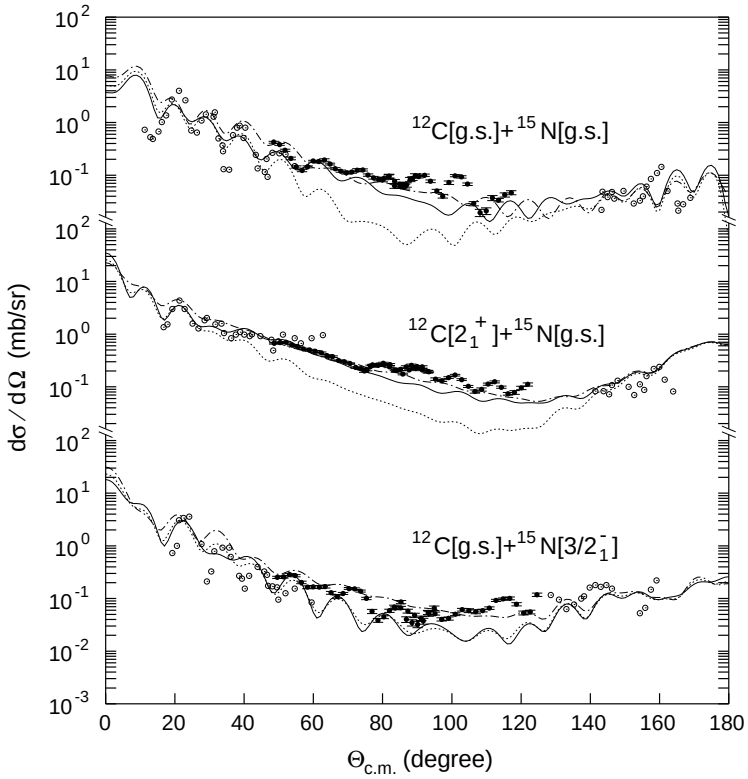

Fig. 6. CC calculations of the cross-sections with the positive deformation lengths for excitations of ^{11}B, applying the spectroscopic amplitudes listed in columns CC-I (solid lines) and CC-II (dot-dashed lines) in table 1, and the calculation omitting the proton transfer processes to the excited states of ^{11}B (dotted lines).

dot-dashed lines in figs. 5 and 6. It should be noted that the values of the spectroscopic amplitude multiplied by the deformation lengths for the individual states are the same as those in CC-I. This implies that the multi-step processes passing through the excited states of ^{11}B have significant effects on the polarization tensors.

To clarify the contributions of the multi-step processes, the CC calculations were made by omitting the proton transfer processes to the excited states of ^{11}B. The calculated results are shown by the dotted lines in figs. 3–6. The calculations give a wrong sign for t_{40} and an out-of-phase oscillation in the angular distribution of t_{20}, when compared with the full CC calculations. The improved reproducibility of the full CC calculations for the cross-section data is also deteriorated by the omission of the proton transfer processes to the excited states of ^{11}B. These results clearly indicate that the multi-step processes involving the excitations of ^{11}B are of crucial importance in the ^{16}O(^{11}B,^{12}C)^{15}N reaction.

5 Summary and conclusion

New experimental data of the polarization tensors t_{20} and t_{40} of ^{12}C[2$_1^+$] were measured for the ^{16}O(^{11}B, ^{12}C[2$_1^+$])^{15}N[g.s.] reaction at 41.25 MeV, for which the DWBA calculation has been pointed out to fail in describing the cross-sections [3–5]. The tensor terms largely deviating from zero were observed, contrary to the one-step DWBA prediction. Following the first example for the ^{16}O(^{13}C,^{12}C[2$_1^+$])^{17}O reaction [6], the present measurement is the second to show the presence of finite ejectile polarization tensor terms unpredictable by the DWBA.

The cross-sections of the reactions to ^{12}C[g. s.] + ^{15}N[g.s.], ^{12}C[2$_1^+$] + ^{15}N[g.s.] and ^{12}C[g.s.] + ^{15}N[3/2$_1^-$] were also measured in the range $48° \leq \Theta_{\rm c.m.} \leq 120°$. The DWBA calculation reasonably reproduces the previous data for the (^{11}B,^{12}C[g.s.]) reactions leading to the ground and 3/2$_1^-$ states of ^{15}N at forward angles [3]. However, the present data extending over a wide angular range have revealed that the DWBA calculation is also unable to describe the measured cross-sections.

The CC calculations taking into account the excitation and reorientation couplings in ^{11}B and ^{12}C were found to reasonably reproduce the polarization tensors of ^{12}C[2$_1^+$] as well as the cross-sections for the transitions to ^{12}C[g.s.]+^{15}N[g.s.], ^{12}C[2$_1^+$]+^{15}N[g.s.] and ^{12}C[g.s.]+^{15}N[3/2$_1^-$]. The multi-step processes involving the excitations of ^{11}B were shown to significantly contribute to the reaction by making a comparison between the calculations with and without introducing these processes.

The angular distributions of the cross-sections of ^{11}B+^{16}O $\rightarrow$^{12}C+^{15}N in wide angular ranges have also been reported at the ^{16}O incident energies of 27–35 MeV [3,18,19]. At these energies, significant discrepancies be-

tween the experiment and the DWBA calculation have not been observed. However, it may be natural to consider that the multi-step processes are also of importance at lower incident energies than in the present investigation (corresponding to the ^{16}O incident energy of 60 MeV). The application of the polarization tensor measurement to the reaction in a wide range of incident energy may shed a new light upon the reaction mechanisms.

The authors wish to thank Mr. Y. Koga and Mr. T. Maeda for their excellent technical support. The present work was partly supported by Grant-in-Aid for Scientific Research (Grant-in-Aid Nos. 08740210, 10440077 and 11640284) of the Japanese Ministry of Education, Science, Sports and Culture.

References

1. R. Bass, *Nuclear Reactions with Heavy Ions* (Springer-Verlag, Berlin, Heidelberg 1980), and references therein.
2. G.R. Satchler, *Direct Nuclear Reactions* (Oxford University Press, 1983), and references therein.
3. U.C. Schlotthauer-Voos, H.G. Bohlen, W. von Oertzen, R. Bock, Nucl. Phys. A **180**, 385 (1972).
4. R.M. DeVries, Phys. Rev. C **8**, 951 (1973).
5. B. Kamys, Z. Rudy, J. Kisiel, E. Kwasniewicsz, H.H. Wolter, Z. Phys. A **342**, 149 (1992).
6. N. Ikeda, F. Nakamura, K. Mizuuchi, T. Sugimitsu, S. Teruyama, T. Okamoto, H. Fujita, S. Morinobu, Eur. Phys. J. A **7**, 491 (2000).
7. F. Petrovich, D. Stanley, L.A. Parks, P. Nagel, Phys. Rev. C **17**, 1624 (1978).
8. P.K. Moffa, Phys. Rev. C **16**, 1431 (1977).
9. H. Amakawa, K.-I. Kubo, Nucl. Phys. A **266**, 521 (1976).
10. S. Cohen, D. Kurath, Nucl. Phys. A **101**, 1 (1967).
11. B.A. Clegg, Nucl. Phys. **38**, 353 (1962).
12. I.J. Thompson, Comput. Phys. Rep. **7**, 167 (1988).
13. M.A.M. Shahabuddin, C.J. Webb, V.R. Edwards, Nucl. Phys. A **284**, 83 (1977).
14. J. Cook, A.K. Abdallah, M.N. Stephens, K.W. Kemper, Phys. Rev. C **35**, 126 (1987).
15. G.H. Fuller, V.W. Cohen, Nucl. Data Tables A **5**, 433 (1969).
16. J. Cook, M.N. Stephens, K.W. Kemper, Nucl. Phys. A **466**, 168 (1987).
17. I. Kohno, S. Nakajima, T. Tonuma, M. Odera, J. Phys. Soc. Jpn. **30**, 910 (1971).
18. R. Bock, M. Groβe-Schulte, W. von Oertzen, Phys. Lett. **22**, 456 (1966).
19. U.C. Schlotthauer-Voos, R. Bock, H.G. Bohlen, H.H. Gutbrod, W. von Oertzen, Nucl. Phys. A **186**, 225 (1972).